Effects of Cleavage on Local Cross-Sectional Stress Distribution in Trench Isolation Structure

Atsushi YAGISHITA, Tomohiro SAITO, Satoshi MATSUDA, and Yukihiro USHIKU

Microelectronics Engineering Laboratories, Toshiba Corporation

1, Komukai Toshiba-cho, Saiwai-ku, Kawasaki 210, Japan

We have taken polarized micro-Raman spectra around the cleaved (011) cross section of trenches embedded in the (100) surface of silicon, and found that the cleavage greatly affects the local cross-sectional stress distribution. That is, the stress distribution measured on the cleaved surface includes serious errors. We found that a three-dimensional stress simulation based on the elastic model is useful in explaining the cleavage effects and determining the local cross-sectional stress distribution without cleavage effects.

1. Introduction

The importance of stress-induced defects in the development of integrated-circuit processes is growing because of the extensive use of trench structures as an isolation technique [1]. Accurate information about stress in the silicon is needed to prevent defect generation. Polarized Raman spectroscopy can give direct information about the distribution of mechanical stresses [2, 3]. We have taken polarized Raman spectra of the (011) cross section of a trench embedded in the (100) surface of a silicon wafer, and found that the experimental results did not always agree with the stress distribution calculated by a finite element method. This issue must be resolved in order to obtain accurate and useful information from the Raman measurements.

In this paper, we show that the major cause of the disagreement is the effects of cleavage and that a three-dimensional stress simulation based on the elastic model is useful in explaining these effects.

2. Experiment

Trenches were made by reactive ion etching on the (100) surface of a silicon wafer. A silicon dioxide film of thickness 850 nm was deposited on these trenches (Fig.1). The sample was annealed for 1 hour at a temperature of 1000 ℃. Polarized Raman spectra of the cleaved (011) cross section of the silicon wafer were taken at room temperature with a 514.5 nm beam from an argon-ion laser using a backscattering geometry. Frequency shifts of the three Raman peaks (R1, R2, and R3) were measured on the A-A' line in (xx) and (xy) configurations in an axis system where the x axis is oriented along the crystallographic direction <0-11>, the y axis along <100>, and the z axis along <011> (Fig.2).

3. Theory

A. Stress model

Due to the viscoelastic behavior of the oxide, the trench structure is expected to be stress-free at the annealing temperature (1000 ℃). As the structure cools, stress is generated in the substrate because of the thermal expansion mismatch between SiO_2 and Si. The thermal strain E_{th} is given by

$$E_{th} = \alpha (T - T_0) \tag{1}$$

where α is the coefficient of thermal expansion, T is the final temperature after cooling (room temperature in this case), and the oxide stress is mostly relieved by viscous flow at a temperature of more than T_0 (about 950 ℃).

The relation between stress S and elastic strain E is given by the following tensor equations:

$$S = D E \tag{2}$$
$$S = (Sxx, Syy, Szz, Sxy, Sxz, Syz)$$
$$E = (Exx, Eyy, Ezz, Exy, Exz, Eyz)$$

where D is the elastic constant. We assume orthotropic elasticity for the Si substrate, and isotropic elasticity for SiO_2. In the case of SiO_2, this is given by the following equations using $\mathscr{E}$ (Young's modulus) and ν (Poisson's ratio):

$$Eyy / Exx = -\nu \tag{3}$$
$$S = \mathscr{E}E. \tag{4}$$

The material constants for components used in the simulation were taken from Ref. 4. Since we assume that only thermal strain exists, then the following constitutive equation can be applied:

$$E_{to} = D^{-1} S + \alpha (T - T_0) \tag{5}$$

where E_{to} is total strain.

B. Raman spectroscopy

Crystal silicon has three active optical Raman modes. These are described by the polarizability tensors R1, R2, and R3, respectively [3]. In the absence of strain, these modes have the same frequency, ω_0 (about $520cm^{-1}$). The frequencies ω_i of the optical phonons in the presence of strain are related to the eigenvalues λ_i of the following secular matrix (ϕ_{ij}) by

$$\lambda_i = \omega_i^2 - \omega_0^2, \quad i = R1, R2, R3.$$

$$(\phi_{ij}) = \begin{bmatrix} pE_{11} + q(E_{22} + E_{33}) & 2rE_{12} & 2rE_{13} \\ 2rE_{12} & pE_{22} + q(E_{33} + E_{11}) & 2rE_{23} \\ 2rE_{31} & 2rE_{32} & pE_{33} + q(E_{11} + E_{22}) \end{bmatrix} \tag{6}$$

The Raman shifts are given by

$$\Delta \omega_i \equiv \omega_i - \omega_0 \fallingdotseq \lambda_i / 2\omega_0. \qquad (7)$$

E_{ij} are the components of the strain tensor E in the axis system where axis 1 is oriented along the <100> crystallographic direction, axis 2 along <010>, and axis 3 along <001>. Also, p, q, and r are deformation potential constants and their values for Si were taken from Ref. 5. When incident and scattered light is polarized in the direction given by the unit vectors e_i and e_s respectively, the scattering efficiency of the Raman signal is given by

$$I = A \sum_j | e_i \cdot Rj \cdot e_s |^2 \qquad (8)$$

where A is a constant and j = 1, 2, 3. In the case of measurements in the (xy) configuration, only the R1 phonon can be observed in the Raman signal backscattered from (011) surface. The R2 and R3 modes contribute to the Raman signal measured in the (xx) configuration.

4. Results and Discussion

We calculated the stress distribution around a single trench structure using a finite element method based on the three-dimensional elastic model described in Section 3 above. The three Raman shifts $\Delta\omega_i$ (i = R1, R2, and R3) were calculated from this stress distribution by using Eq. (7). A comparison of these simulated results with the experimental measurements was made for the three Raman shifts, rather than the six stress components, because of the difficulty of measuring all stress components. First, we calculated the stress distribution without the effects of cleavage. That is, the cleaved cross section was assumed to be a symmetrical plane. Figures 3 (a) and (b) show the distribution of horizontal (Sxx) and vertical (Syy) components of stress around the trench, respectively. Since the thermal expansion coefficient of silicon is greater than that of silicon dioxide, Sxx is compressive (about -120 MPa) and Syy is tensile (about 100 MPa) near the sidewall of the trench. On the other hand, the Szz component is relatively small, as shown in Fig.3(c). We calculated the three Raman shifts from these stress (or strain) components and compared them with the experimental results. We found that they disagreed (Fig.4).

In order to clarify the cause of this disagreement, we next calculated the stress distribution including the effects of cleavage. That is, the cleaved cross section was assumed to be a freely mobile plane. Note that the simulation results in the two cases considered below are exactly the same, because the elastic model is used. Case 1: cooling down after cleavage; and case 2: cooling down before cleavage. Figures 5 (a), (b), and (c) show the Sxx, Syy, and Szz components of stress, respectively. The Syy component is relaxed on the cleaved surface and tensile stress appears in the Szz component near the silicon/silicon dioxide interface. These simulated results prove that the cleavage greatly affects the local

cross-sectional stress distribution. In this case, the calculated Raman shifts coincide well with the experimental data (Fig.6).

Finally, we consider the relative contributions of each of the six stress components to the Raman shifts. In the trench structure, the shear stress components (Sxy, Syz, Szx) increase sharply around the trench corners and are relatively small in other regions. Therefore, the three normal components (Sxx, Syy, Szz) are important in most areas measured in this work. Furthermore, without cleavage, the Szz component is also small (Fig.3) and only the Sxx and Syy components are important. However, the results with cleavage effects, as mentioned above, show that the relative contributions of each of the three normal components to the total stress (or Raman shifts) are comparable and that none of them can be ignored. It is impossible to convert the observed two Raman shifts into the three stress components. Therefore, when we consider the local cross-sectional stress distribution on the cleaved surface, it is necessary to use the Raman shifts for a comparison of the simulated results with the experimental results. However, if polarized off-axis Raman spectroscopy [6] were used, all six stress components could be uniquely determined and the comparison could be performed using the stress components.

5. Conclusion

Polarized micro-Raman spectroscopy is a powerful technique for the estimation of an anisotropic stress in silicon devices. However, the stress distribution measured on the cleaved surface greatly differs from the original stress distribution without cleavage. We found that a three-dimensional stress simulation based on the elastic model is useful for explaining the effects of cleavage and determining the local cross-sectional stress distribution without cleavage effects. That is, a combination of Raman measurements and a stress simulation is an effective means of estimating the local cross-sectional stress distribution. This technique will be useful in designing low-stress devices and processes which reduce defect generation.

6. Reference

[1] P.M.Fahey, S.R.Mader, S.R.Stiffler, R.L.Mohler, J.D.Mis, and J.A.Slinkman, IBM J. Res. Develop. **36** (1992) 158

[2] M.Yoshikawa, M.Maegawa, G.Katagiri, and H.Ishida, J. Appl. Phys. **78** (1995) 941

[3] I.De Wolf, J.Vanhellemont, A.Romano-Rodriguez, H.Norstrom, and H.E.Maes, J. Appl. Phys. **71** (1992) 898

[4] S.Matsuda, C.Yoshino, H.Nakajima, K.Inou, S.Yoshitomi, Y.Katsumata, and H.Iwai, IEDM Tech. Digest. (1994) p.885

[5] F.Cerdeira, C.J.Buchenauer, F.H.Pollak, and M.Cardona, Phys. Rev. B**5** (1972) 580

[6] G.H.Loechelt, N.G.Cave, and J.Menendez, Appl. Phys. Lett. **66** (1995) 3639
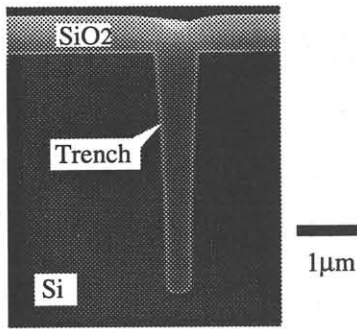
Fig.1 Cross-sectional SEM micrograph of the trench structure
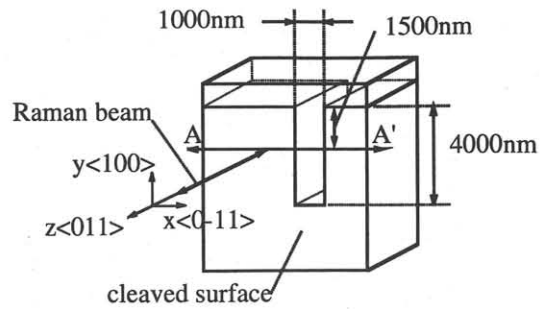
Fig.2 Schematic diagram for the structure of the (011) cross-section of the trench
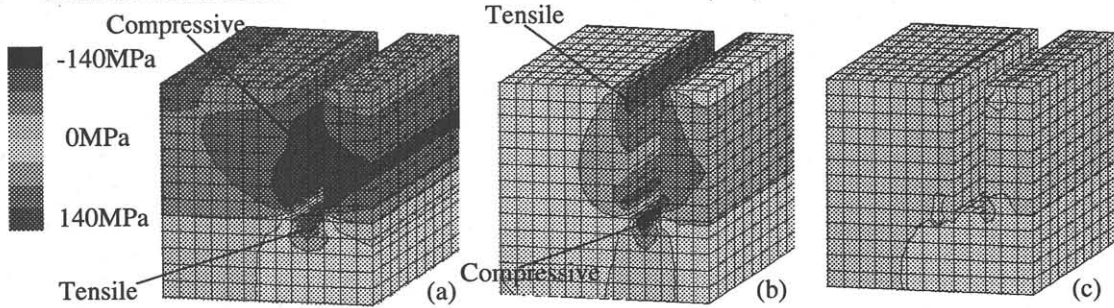
Fig.3 Calculated stress distributions of (a) Sxx, (b) Syy, and (c) Szz without cleavage effects
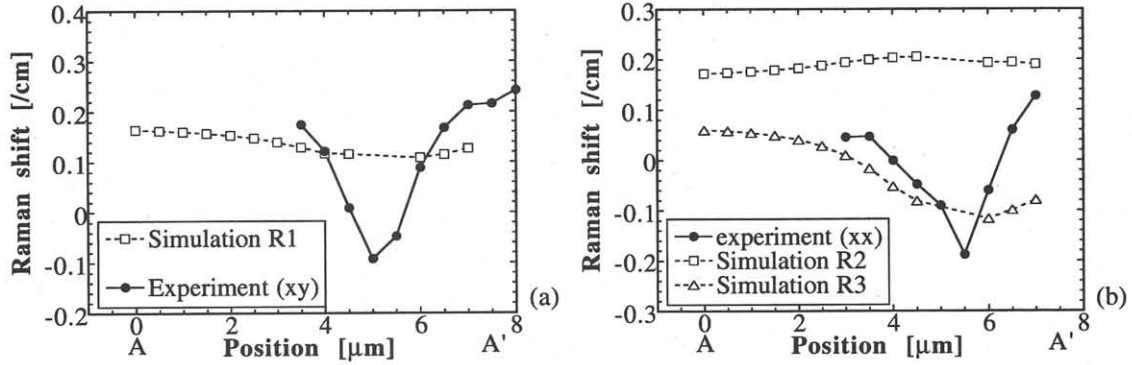
Fig.4 (a) Raman shift measured in (xy) configuration, (b) Raman shift measured in (xx) configuration, and simulated Raman shift (R1, R2, R3) without cleavage effects
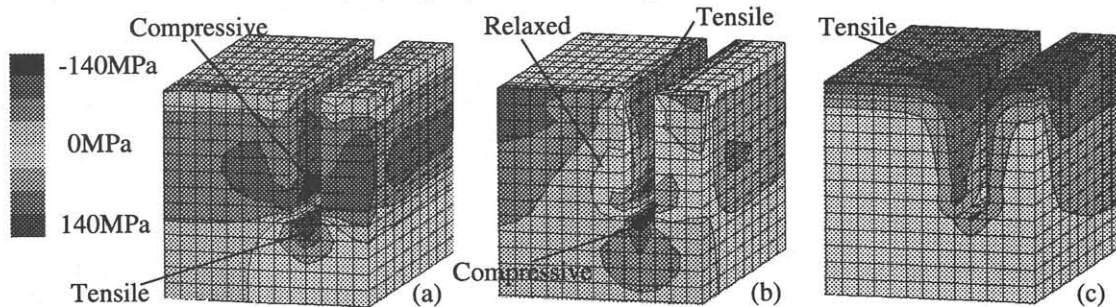
Fig.5 Calculated stress distributions of (a) Sxx, (b) Syy, and (c) Szz with cleavage effects
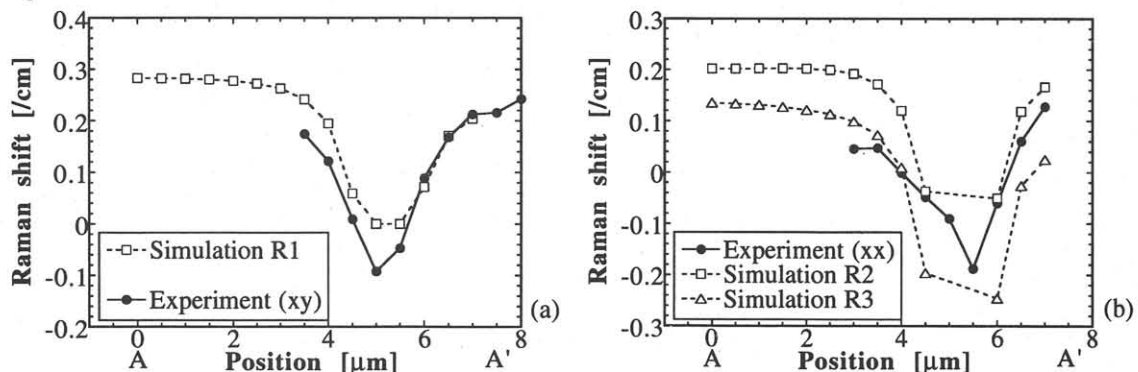
Fig.6 (a) Raman shift measured in (xy) configuration, (b) Raman shift measured in (xx) configuration, and simulated Raman shift (R1, R2, R3) with cleavage effects